Synthesis and Characterization of $Sr_3FeMoO_{6.88}$: An Oxygen-Deficient 2D Analogue of the Double Perovskite Sr_2FeMoO_6

Gabriel M. Veith,[†,‡] Martha Greenblatt,*[,‡] Mark Croft,[§] K. V. Ramanujachary,[∥] J. Hattrick-Simpers,[∥] Samuel E. Lofland,[∥] and Israel Nowik[¶]

Department of Chemistry and Chemical Biology, Rutgers, The State University of New Jersey, Piscataway, New Jersey 08854, Department of Physics and Astronomy, Rutgers, The State University of New Jersey, Piscataway, New Jersey 08854, Department of Chemistry and Physics, Rowan University, Glassboro, New Jersey 08028, and [4]Racah Institute of Physics, The Hebrew University, Jerusalem, 91904 Israel

Received July 16, 2004. Revised Manuscript Received March 8, 2005

We have prepared $Sr_3FeMoO_{6.88(1)}$, an oxygen-deficient two-dimensional analogue of the double perovskite Sr_2FeMoO_6, and have investigated its structure and physical properties. According to powder X-ray and neutron diffraction data, $Sr_3FeMoO_{6.88}$ adopts the tetragonal $n = 2$ Ruddlesden−Popper structure (space group *I*4/*mmm*) with a completely disordered B-cation distribution and oxygen vacancies occurring preferentially at the axial O1 sites between the perovskite layers. X-ray absorption near-edge spectroscopy and Mössbauer data are consistent with trivalent Fe and mixed (4+/5+) Mo oxidation state. The compound is semiconducting, showing an intrinsic magnetic transition at ∼85 K and an additional upturn in the magnetic susceptibility at ∼270 K, the latter is associated with intergrowth defects. An appreciable magnetoresistance, reaching the value of ∼−15% at 5 K and 5 T is also observed

Introduction

Since the first reports of large negative magnetoresistance (MR) in mixed valent perovskite manganites,[1] $Ln_{1-x}A_xMnO_3$ (Ln = rare earth, A = divalent cation),[2] there has been a great deal of research to understand the fundamental mechanism of MR and to discover new compounds with large MR. Under certain critical conditions, some manganites undergo a transition from a paramagnetic insulator (PMI) to a ferromagnetic metal (FMM) at low temperatures,[2] and their resistance decreases dramatically in an applied magnetic field near the PMI−FMM transition. These compounds are envisioned for possible applications including sensors and read heads in computer hard drives. However, presently, the large applied magnetic fields and low-operating temperatures required for the onset of large MR render these materials impractical for device applications.

Recently, attempts have been made to improve and understand the properties of manganites by investigating the perovskite-related, low-dimensional Ruddlesden−Popper (RP) phases.[3] The crystal structure of RP phases $[AO(ABO_3)_n]$ consists of n number of ABO_3 perovskite layers, with $n = 1, 2, 3, ...\infty$, separated by insulating rock-salt layers, AO.[4,5] The introduction of the insulating AO layer between the conducting perovskite-like layers results in substantial two-dimensional (2D) character. In the quasi-low-dimensional (LD) RP-systems, electronic correlations are enhanced and the magnetotransport behavior is expected to be interesting because of anisotropic transport and magnetic exchange interactions. Indeed, the $n = 2$ RP phase $Sr_{1.8}La_{1.2}Mn_2O_7$ was reported to exhibit a large MR, >200%, at a relatively low magnetic field (0.3 T) at 126 K.[6] This MR is considerably larger than values reported for manganite perovskites of similar manganese oxidation state and applied magnetic field, 3000% versus 110%, albeit at much lower temperatures.[7]

The search for new materials with large MR at low fields and near room temperature has also included ordered double perovskites, $A_2BB'O_6$, where A is a divalent cation and B and B′ are two different transition-metal ions. The double perovskite Sr_2FeMoO_6, first reported in 1963 by Patterson et al.,[8] is a semimetal with an ordered array of the B cations $Fe^{3+}(d^5)$ and $Mo^{5+}(d^1)$, which order ferrimagnetically at 410 K.[9] More recently, Kobayashi et al. reported a large MR for Sr_2FeMoO_6 at low fields.[10] In this paper, we report the synthesis and characterization of the $n = 2$ RP phase Sr_3-

* Corresponding author e-mail: greenblatt@rutchem.rutgers.edu.
† Present address: Oak Ridge National Laboratory, Oak Ridge TN, 37831.
‡ Department of Chemistry and Chemical Biology, Rutgers, The State University of New Jersey.
§ Department of Physics and Astronomy, Rutgers, The State University of New Jersey.
∥ Rowan University.
¶ The Hebrew University.

(1) Kusters, R. M.; Singleton, J.; Keen, D. A.; McGreevy, R.; Hayes, W. *Physica B* **1989**, *155*, 362.
(2) Raveau, B.; Maignan, A.; Martin, C.; Hervieu, M. *Chem. Mater.* **1998**, *10*, 2641.
(3) Battle, P. D.; Rosseinsky, M. J. *Cur. Opin. Solid State Mater. Sci.* **1999**, *4*, 163.
(4) Ruddlesden, S. N.; Popper, P. *Acta Crystallogr.* **1958**, *11*, 54.
(5) Ruddlesden, S. N.; Popper, P. *Acta Crystallogr.* **1957**, *10*, 538.
(6) Moritomo, Y.; Tomioka, Y.; Asamitsu, A.; Tokura, Y.; Matsui, Y. *Phys. Rev. B* **1995**, *51* (5), 3297.
(7) Moritomo, Y.; Asamitsu, A.; Kuwahara, H.; Tokura, Y. *Nature* **1996**, *380*, 141.
(8) Patterson, F. K.; Moeller, C. W.; Ward, R. *Inorg. Chem.* **1963**, *1*, 196.
(9) Chmaissem, O.; Kruk, R.; Dabrowski, B.; Brown, D. E.; Xiong, X.; Kolesnik, S.; Jorgensen, J. D.; Kimball, C. W. *Phys. Rev. B.* **2000**, *62* (21), 14197.
(10) Kobayshi, K.-I.; Kimura, T.; Sawada, H.; Terakura, K.; Tokura, Y. *Nature* **1998**, *395*, 677.

10.1021/cm048839r CCC: $30.25
Published on Web 04/15/2005

$FeMoO_{7-\delta}$: a compound expected to share the properties of RP manganites and double perovskites.

Experimental Section

Sr_3FeMoO_7-δ was synthesized from stoichiometric mixtures of SrO (prepared by decomposing SrC_2O_4, Alfa, 95% Assay, at 1300 °C for 4 h in air), Fe_2O_3 (Fisher Certified, 99+%), Mo (Alfa, 99.95%, −100 mesh), and MoO_3 (Alfa, 99.95%) by solid-state reaction. Strontium oxalate was used as a starting reagent since it completely decomposes into SrO at 950 °C (according to TGA and X-ray measurements). Mo was checked by powder X-ray diffraction prior to use to ensure that no oxides were present. All reagents were stored and thoroughly ground in an argon-filled drybox to prevent reaction of SrO with water to yield $Sr(OH)_2$. The mixed powders were pressed into pellets and sealed in evacuated quartz tubes with a pressure of $\sim 10^{-4}$ Torr. Samples were heated at 550 °C for 24 h and then slowly ramped to 1100 °C over a period of 8 h. After 24 h at 1100 °C, the samples were quenched to room temperature by removing the tube from the furnace. The samples were reground in air, pressed into pellets, sealed in quartz tubes, and sintered at 1200 °C for 40 h and then quenched to room temperature. Chemical analysis was preformed on randomly selected crystallites to verify homogeneity of the samples with an EDAX brand energy-dispersive X-ray spectroscopy (EDS) device attached to a JEOL JSM-840 scanning electron microscope (SEM). Thermogravimetric analysis (TGA) was performed with a TA Instrument 2050 thermal analyzer. Samples were ramped at 2°/min to a final temperature of 400−600 °C, and they were held there for 8 h.

Powder X-ray diffraction (PXD) data of the product were collected with a Scintag PAD V diffractometer using Cu−K_α radiation. Data were collected over a range of $4° \leq 2\theta \leq 120°$, with a step size of 0.02°. Time-of-flight neutron powder diffraction data were collected at room temperature on the general purpose powder diffractometer (GPPD) beam line at the intense pulsed neutron source (IPNS) at Argonne National Laboratory with the sample mounted in a sealed cylindrical vanadium can. The program GSAS[11] was used for the final Rietveld refinement of the high-resolution backscattering data collected on Bank 1, covering the range $0.30 \text{ Å} \leq d \leq 3.00 \text{ Å}$.

Magnetic susceptibility (χ) measurements were carried out with a Quantum Design MPMS-XL SQUID magnetometer in a variety of applied fields up to 70 kOe. Zero-field-cooled (ZFC) data were collected on heating from 5 to 400 K while field-cooled (FC) data were collected on the subsequent cooling. Temperature-dependent resistivity (ρ) was measured with four-point probes in the bar geometry. MR was measured by holding the temperature constant and varying the magnetic field between 0 and 5 T. High-field (up to 70 kOe) isothermal magnetization curves were measured in a Quantum Design Physical Property Measurement System (PPMS). MR was calculated with the equation

$$\%\text{MR} = (\rho_H - \rho_0)/\rho_0 \times 100$$

where ρ_H is the resistance of the compound in a magnetic field of H and ρ_0 is the resistance without a magnetic field.

The X-ray absorption near-edge spectra (XANES) were obtained on beam line X-19A at the Brookhaven National Synchrotron Light Source with a double crystal Si(111) monochromator. The Mo L-edge measurements were made in both the fluorescence and electron yield modes with the data being displayed in the latter mode. The relative energies between various spectra were established by comparison with standard spectra run bracketing the sample scan. In general, the relative accuracy of the energy for the Mo L-edges is better than ±0.1 eV. The Fe−K edge measurements were performed in the transmission and fluorescence modes with the data being displayed in the latter mode. A simultaneous standard, run with all Fe spectra, enables a relative energy calibration of about ±0.03 eV. All spectra were normalized to unity step in the absorption coefficient from well below to well above the edge.

Mössbauer studies were performed with a ^{57}Co:Rh source (50 mCi) and a conventional constant acceleration Mössbauer drive. The spectra of $Sr_3FeMoO_{6.88}$ at 90 and 300 K were analyzed and fitted to a distribution of three quadrupole doublets with differing isomer shifts. The 4.2 K spectrum was fitted to a distribution of magnetic hyperfine fields, isomer shifts, and quadruple splittings.

Results and Discussion

1. Synthesis and Preliminary Characterization. While our initial goal was to synthesize stoichiometric Sr_3FeMoO_7, the fully oxygenated phase could not be prepared. Numerous synthesis attempts resulted in products with a white amorphous surface coating while the inside of the pellets contained a mixture of Sr_3MoO_6 and an $n = 2$ RP-like phase. Since it has been established that many $n = 2$ RP phases form with oxygen deficiencies,[12−18] we attempted to synthesize an oxygen-deficient sample, $Sr_3FeMoO_{6.5}$, using the same method described for Sr_3FeMoO_7. This strategy yielded a single-phase $n = 2$ RP compound which is black, but which decomposes within a few months in air, according to PXD data. To verify the oxygen content, TGA analysis was performed under reducing conditions. However, the TGA results were inconclusive because the compound decomposes around 600 °C. EDS results indicated a homogeneous distribution of Fe and Mo within the sample, as well as confirmed that the cation composition is equal to the nominal within experimental error.

2. Crystal Structure. To estimate the concentration and location of oxygen vacancies time-of-flight (TOF), powder neutron diffraction (PND) data were collected. The diffraction patterns can be completely indexed with the *I*-centered tetragonal lattice with no systematic extinctions, and no evidence for symmetry lowering was observed. Consequently, Rietveld refinements of the structure were carried out in space group *I*4/*mmm* (no. 139), corresponding to the ideal RP structure without any ordering or octahedral tilts, with both the PXD and PND data. Anisotropic atomic displacement parameters (ADP) were used which resulted in a significant improvement of the fit over isotropic ADPs ($\chi^2 = 5.24$, wRp = 5.82, Rp = 3.73, vs $\chi^2 = 6.20$, wRp = 6.33, Rp = 4.22). No evidence of Fe/Mo ordering was

(11) Larson, A. C.; von Dreele, R. B.; Los Alamos National Laboratory Report No. LA-UR-86-748 ed., 1987.

(12) Veith, G. M.; Chen, R.; Popov, G.; Croft, M.; Shokh, Y.; Nowik, I.; Greenblatt, M. *J. Solid State Chem.* **2002**, *166* (2), 292.
(13) Veith, G. M.; Fawcett, I. D.; Greenblatt, M.; Croft, M.; Nowik, I. *Int. J. Inorg. Mater.* **2000**, *2*, 513.
(14) Fawcett, I. D.; Veith, G. M.; Greenblatt, M.; Croft, M.; Nowik, I. *J. Solid State Chem.* **2000**, *155*, 96.
(15) Mitchell, J. F.; Millburn, J. E.; Medarde, M.; Short, S.; Jorgensen, J. D.; Fernández-Díaz, M. T. *J. Solid State Chem.* **1998**, *141*, 599.
(16) Dann, S. E.; Weller, M. T. *J. Solid State Chem.* **1995**, *115*, 499.
(17) Dann, S. E.; Weller, M. T.; Currie, D. B. *J. Solid State Chem.* **1992**, *97*, 179.
(18) Battle, P. D.; Branford, W. R.; Mihut, A.; Rosseinsky, M. J.; Singleton, J.; Sloan, J.; Spring, L. E.; Vente, J. F. *Chem. Mater.* **1999**, *11*, 674.

Table 1. Structural Parameters and Bond Lengths (Å) and Angles (deg) for $Sr_3FeMoO_{6.88(1)}$[a]

atom	site	x	y	z	occupancy	$U_{11} = U_{22}$[b] (Å^2)	U_{33} (Å^2)
Sr1	2*b*	0	0	$^1/_2$	1	0.0119(4)	0.0158(8)
Sr2	4*e*	0	0	0.3150(1)	1	0.0109(3)	0.0100(5)
Fe/Mo	4*e*	0	0	0.0989(1)	0.500/0.500(3)	0.0049(2)	0.0151(4)
O1	2*a*	0	0	0	0.876(10)	0.0157(7)	0.0096(11)
O2	8*g*	0	$^1/_2$	0.0946(1)	1	0.0110(3)	0.0197(4)
O3	4*e*	0	0	0.1960(1)	1	0.0147(4)	0.0077(6)

Sr1−O1	2.78293(1) × 4	O1−Fe/Mo−O2	87.45(5)
Sr1−O2	2.7600(8) × 8	O2−Fe/Mo−O2	89.89(4)
mean Sr1−O	2.7676	O3−Fe/Mo−O2	92.55(5)
Sr2−O2	2.7017(13) × 4	Fe/Mo−O1−Fe/Mo	180.00(0)
Sr2−O3	2.4367(18) × 1	Fe/Mo−O2−Fe/Mo	174.90(9)
Sr2−O3	2.79191(15) × 4		
mean Sr2−O	2.7123		
Fe/Mo−O1	2.0230(10) × 1		
Fe/Mo−O2	1.96978(7) × 4		
Fe/Mo−O3	1.9872(15) × 1		
mean Fe/Mo−O	1.9816		

[a] Space group, *I*4/*mmm*; $a = 3.9356(1)$ Å; $c = 20.4667(1)$ Å; $\chi^2 = 5.241$; wRp = 0.0582; Rp = 0.0373; 44 variables. [b] $U_{11} = U_{22}$ for all atoms except O2; $U_{22}(O2) = 0.0041(3)$.

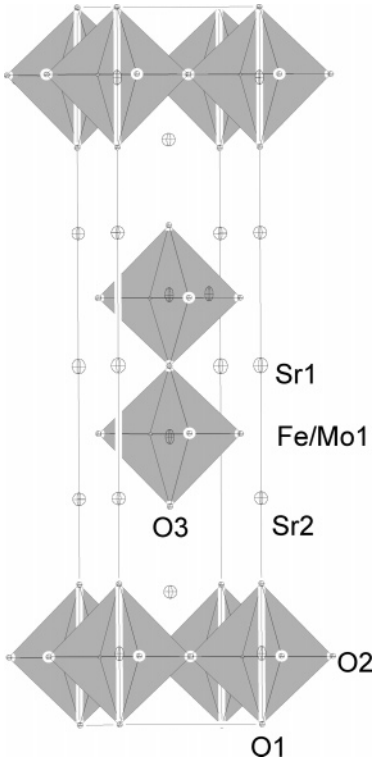

Figure 1. Structure of the $n = 2$ RP phase $Sr_3FeMoO_{6.88}$.

observed in either the PXD or the PND data, and refinement of the fractional occupancies resulted in a 1:1 Fe:Mo ratio. Refinement of the oxygen occupancies indicates that the oxygen vacancies preferentially occur between the two perovskite layers at the O1 site (Table 1, Figure 1), consistent with reported neutron results on similar RP compounds.[12−14,16−18] The refined oxygen occupancies for O2 and O3 sites were close to 1.00 (0.98(5) and 0.99(5), respectively) and were fixed to full occupancy for the final refinement. The as-refined oxygen stoichiometry is significantly higher than the nominal value (6.5) and results in a $Sr_3FeMoO_{6.88(1)}$ composition. Thus, it appears that during the synthesis the sample incorporated additional oxygen, either

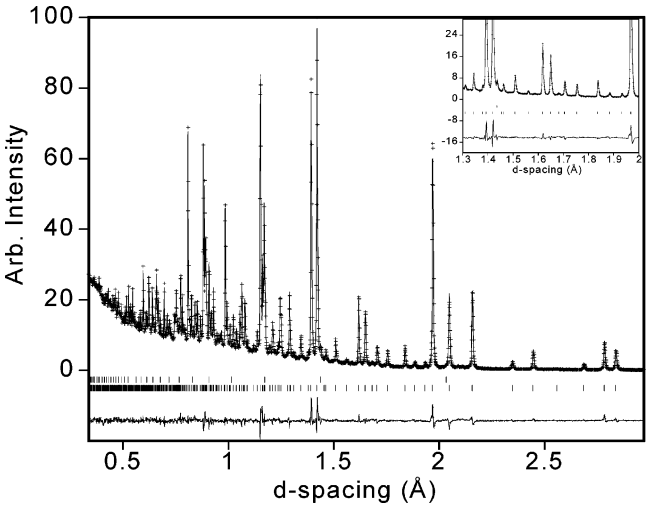

Figure 2. Powder neutron diffraction pattern of $Sr_3FeMoO_{6.88}$; observed (+), calculated (solid line), and allowed reflections (tics) of Fe (top tics) and $Sr_3FeMoO_{6.88}$ (bottom tics) and difference plot (bottom). Inset: Expanded view of the PND pattern of $Sr_3FeMoO_{6.88}$.

from the quartz tube or from ambient air during the regrindings. The neutron diffraction pattern of $Sr_3FeMoO_{6.88}$ along with the fitted profile and the difference plot is shown in Figure 2. The refined lattice parameters, atomic positions, ADPs, relevant bond lengths, and angles are listed in Table 1. Fe metal impurity (*Im*3*m* − $a = 2.872$Å, with March−Dollase preferred orientation correction) was introduced into the refinement as a second phase, and its refined fraction was 2.0(1)%. Further attempts to improve the refinement by introducing additional impurity phases such as Sr_2FeMoO_6 (double perovskite) and Sr_4FeMoO_8 ($n = 1$) failed to improve the fitting of the data and therefore were excluded for the final refinement. There are small errors in the intensities of the refined model. Since the ADPs are reasonable, the errors could result from stacking faults as they are typically observed in the RP phases.[19]

The oxygen deficiency manifests itself in the $Sr_3FeMoO_{6.88}$ structure in several ways. The Fe/Mo atoms are displaced away from the O1 vacancy resulting in an axial Fe/Mo−O1 bond (2.023 Å) considerably longer than the other five (1.970−1.987 Å). The "in-plane" Fe/Mo−O(2)−Fe/Mo bond angle is 174.9°, and the deviation from the ideal 180° value is caused by the Fe/Mo atom shift from the center of the octahedron. Finally, local disorder (i.e., the O1 site is either occupied or empty) could possibly manifest itself in the anisotropy of the Fe/Mo ADPs (with elongation along the *c* direction, $U_{33}/U_{11} \sim 3.1$). These results also show that one out of every eight oxygen atoms is missing at this particular site (2*a*). These missing oxygens would result in ∼12% of the Fe or Mo to occupy a five-coordinate pyramidal site. There was no manifestation of vacancy ordering in the neutron data.

The average Fe/Mo−O bond lengths, 1.982 Å, are close to those reported for Sr_2FeMoO_6,[9] 1.973−1.978 Å. The slight increase in the M−O bond lengths is attributed to the presence of some Mo^{4+} (with effective ionic radius of 0.79 Å vs 0.75 Å for Mo^{5+})[20,21] in $Sr_3FeMoO_{6.88}$. Justification for

(19) Sloan, J.; Battle, P. D.; Green, M. A.; Rosseinsky, M. J.; Vente, J. F. *J. Solid State Chem.* **1998**, *138*, 135.

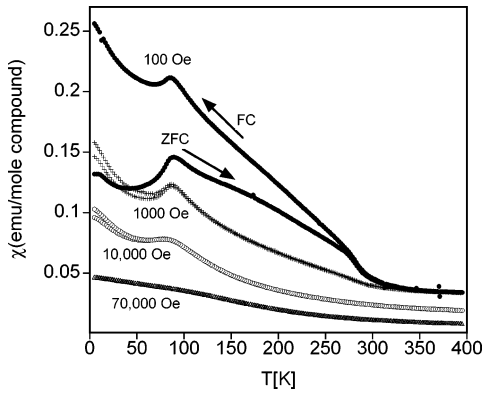

Figure 3. Temperature-dependent susceptibility, χ, of $Sr_3FeMoO_{6.88}$ measured at 0.01, 0.1, 1, and 7 kOe.

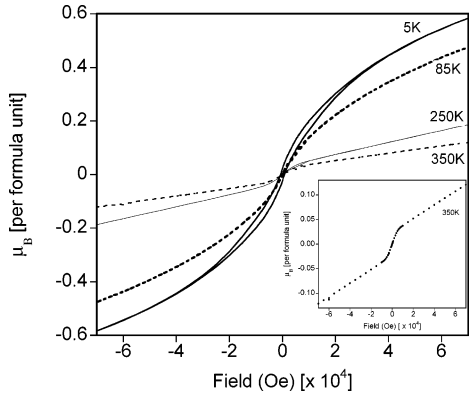

Figure 4. Magnetization as a function of field for $Sr_3FeMoO_{6.88}$ at 5, 85, 250, and 350 K. There is noticeable hysteresis at 5 K. (Inset, expanded magnetization data collected at 350 K).

invoking Mo in 4+ formal oxidation state will be given by the Mössbauer, XANES, and magnetic results presented later.

3. Magnetic Susceptibility. The temperature-dependent magnetic susceptibility, χ, of $Sr_3FeMoO_{6.88}$ in Figure 3 shows significant field dependence. Nevertheless, in all sets of data, a transition at 85 K is observed (the transition measured at 70 kOe is too small to be seen on this scale). There is also a clear upturn in χ around 270 K, the origin of which is discussed below. The overall magnitude of the susceptibility decreases with increasing field, while the deviations between the FC and ZFC data decrease with field strength. Curie−Weiss (CW) fit of the high-temperature data, 330−400 K, resulted in unrealistically large Curie and Weiss constants.

M−H loops measured at 350 K revealed a small ferromagnetic (FM) component at fields smaller than 70 kOe and a nearly linear paramagnetic signal at higher fields (inset Figure 4). This behavior can be attributed to the presence of a small amount of Fe metal impurity, consistent with the PND findings. Since the Curie temperature of Fe metal is high (∼1043 K), its contribution to the total magnetization should not vary over the range of temperatures considered here, as verified by recording M−H loops at several temperatures in the range 300−350 K. The presence of a small amount of Fe is not unique to our samples: there are reports of an Fe impurity in the double perovskite Sr_2FeMoO_6,[22−24] and we also have observed such an impurity in

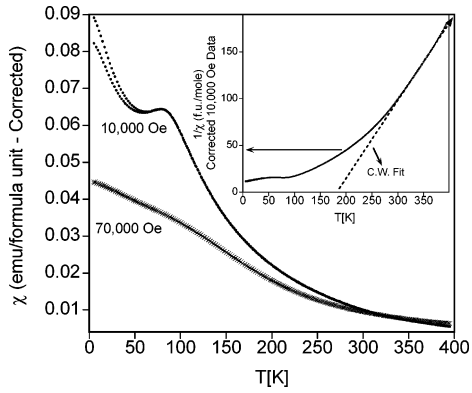

Figure 5. Magnetic susceptibility data for $Sr_3FeMoO_{6.88}$ ($H = 10$ and 70 kOe) corrected for the FM impurity. (Inset: Plot of $1/\chi$ vs T plot for the corrected $H = 10$ kOe susceptibility data along with extrapolated plot of Curie−Weiss fit).

Y_2FeMoO_7.[25] Fe impurities can readily form in excessive reducing conditions.[24] The fraction of Fe estimated from the magnetization data is 1.6%, which is in good agreement with the value refined from the PND data.

The calculated contribution of Fe to the magnetic susceptibility was subtracted from the 10 000 and 70 000 Oe data; the corrected susceptibility data are shown in Figure 5, and CW fit is shown in the inset. At high temperatures, $T > 300$ K, the corrected data overlap well; however, the CW fit fails below the magnetic upturn at $T \sim 270$ K. The Curie (C) and Weiss (θ) constants obtained from the CW fit of the high-T region are 1.19 emu/mol K and 182 K, respectively. The observed effective paramagnetic moment (μ_{eff}) of 3.08 μ_B is significantly lower than the theoretically expected spin-only value of 6.26 μ_B [assuming 12% Mo^{4+} (d^2), 38% Mo^{5+} (d^1), and 50% Fe^{3+} (d^5)] and that of the magnetic moment of 4.20 μ_B reported for Sr_2FeMoO_6.[23] The Weiss constant is positive indicating that the dominant magnetic interactions are FM, similar to those reported for Sr_2FeMoO_6 [$\theta = 439$ K], although the magnitude of the interactions is significantly smaller. The hysteresis seen at 5 K in the M−H loop (Figure 5) is consistent with a presence of a FM component, far exceeding the small contribution expected from Fe impurity.

The upturn in the magnetic susceptibility around 270 K is tentatively associated with intergrowth type defects (i.e., areas where $n \neq 2$) which order ferromagnetically into local clusters. The Mössbauer data (see below) is in favor of this interpretation. Such intergrowths have been observed previously for the $n = 2$ manganite $Sr_{1.8}La_{1.2}Mn_2O_7$ by transmission electron microscopy.[26,27] $Sr_3FeMoO_{6.88}$ undergoes a magnetic transition at $T \sim 85$ K. The clear hysteresis in the M(H) curves at temperatures below 85 K indicates the

(20) Shannon, R. D.; Prewitt, C. T. *Acta Crystallogr.* **1969**, *B25*, 925.
(21) Shannon, R. D. *Acta Crystallogr.* **1976**, *A32*, 751.
(22) Causa, M. T.; Butera, A.; Tovar, M.; Fontcuberta, J. *Physica B* **2002**, *320* (1), 79.
(23) Navarro, J.; Balcells, L.; Martínez, B.; Fontcuberta, J. *J. Appl. Phys.* **2001**, *89* (11), 7684.
(24) Navarro, J.; Frontera, C.; Rubi, D.; Mestres, N.; Fontcuberta, J. *Mater. Res. Bull.* **2003**, *38*, 1477.
(25) Veith, G. M.; Lobanov, M. V.; Emge, T. J.; Greenblatt, M.; Croft, M.; Stowasser, F.; Hadermann, J.; Van Tendeloo, G. *J. Mater. Chem.* **2004**, *14* (10), 1623.
(26) Bader, S. D.; Osgood, R. M., III; Miller, D. J.; Mitchell, J. F.; Jiang, J. S. *J. Appl. Phys.* **1998**, *83* (11), 6385.
(27) Potter, C. D.; Swiatek, M.; Bader, S. D.; Argyriou, D. N.; Mitchell, J. F.; Miller, D. J.; Hinks, D. G.; Jorgensen, J. D. *Phys. Rev. B* **1998**, *57* (1), 72.

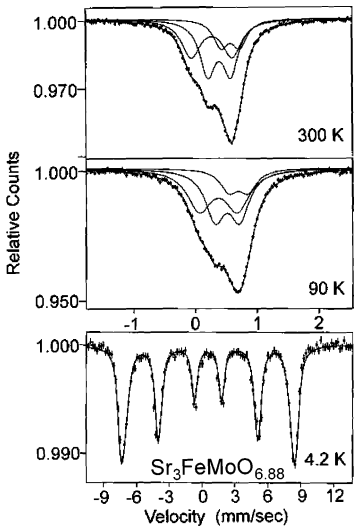

Figure 6. Mössbauer spectra of $Sr_3FeMoO_{6.88}$ measured at 300, 90, and 4.2 K.

presence of an FM component. However, the absence of saturation in the magnetization data and the relatively small value of the magnetic moment (0.57 μ_B at 7 T; Figure 4) indicate that this magnetic structure is not a simple FM.

4. Mössbauer Study. The Mössbauer spectra of $Sr_3FeMoO_{6.88}$ at 90 and 300 K, Figure 6, exhibit three broadened line quadrupole doublets corresponding to inequivalent iron sites, consistent with a random distribution of iron neighbors. The hyperfine interaction parameters, isomer shift (0.3−0.5 mm/s), and quadrupole splitting (0.3−0.8 mm/s) at 300 K fall in a narrow range and indicate that all the iron ions are basically trivalent, differing only in nearest-neighbor local environments. In Sr_2FeMoO_6, the room-temperature isomer shift of 0.55−0.58 [ref 28] was used to argue that the average Fe valence (a continuous variable in these systems with substantial covalency) had been pulled somewhat below 3+. The isomer shift of $Sr_3FeMoO_{6.88}$ is consistent with an Fe valence somewhat larger than that in Sr_2FeMoO_6 consistent with the Fe−K edge results discussed below.

The spectrum at 4.2 K exhibits a single magnetic sextet with a magnetic hyperfine field of 504(5) kOe and isomer shift of 0.5 mm/s, providing stronger evidence that the iron ions are indeed all trivalent. The absorption lines in the 4.2 K spectrum, Figure 6, are significantly broadened, because of the spread in isomer shifts and quadrupole interactions observed in the spectra above the magnetic ordering temperature of the material. The absorption lines at 90 K are slightly broader than those at 300 K, a precursor of the 85 K magnetic transition. The absence of magnetic splitting in the 90 K Mössbauer spectrum suggests that the 270 K magnetic susceptibility upturn is due to extrinsic, ($n \neq 2$ type) intergrowth origin.

5. XANES Study. Figure 7 shows the Fe−K edge spectra of the $Sr_3FeMoO_{6.88}$ sample along with a series of standard iron oxide spectra. Although the K-edge spectra of 3d transition-metal oxides can exhibit strong structural differences, a nominal chemical shift for such compounds can be

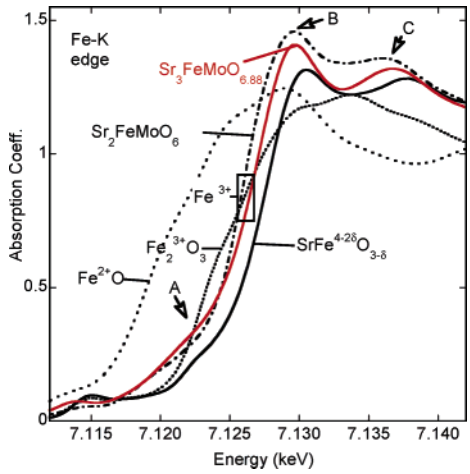

Figure 7. Fe−K edge XANES data.

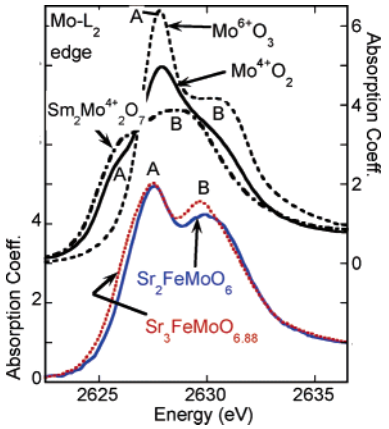

Figure 8. Mo−L_2 edge XANES data.

estimated by their energy at the absorption coefficient of $\mu \sim 0.8$ of the edge step.[29−31] The Fe^{2+} (FeO) and ~Fe^{4+} $SrFeO_{3-\delta}$ spectra clearly bracket the spectra of $Sr_3FeMoO_{6.88}$ at lower and higher energies, respectively. The box in the figure emphasizes the proximity of the nominal chemical shifts of the $Sr_3FeMoO_{6.88}$ spectra with those of Fe_2O_3 and $SrFeMoO_6$ supporting a nominal Fe^{3+} oxidation state. Interestingly, the $Sr_3FeMoO_{6.88}$ spectrum is shifted slightly to higher energy than $Sr_3FeMoO_{6.88}$ suggesting a somewhat higher valence in the former (as indicated by the Mössbauer isomer shift values noted above).

Figures 8 and 9 show the Mo L_3- and L_2-edges for $Sr_3FeMoO_{6.88}$ along with a series of molybdenum standard compounds. Since the A and B features, in both Figures 8 and 9, involve transitions into t_{2g} and e_g final states, respectively, their relative intensity provides evidence as to the hole count in these orbitals.[30,31] Specifically, the intensity of the A feature increases relative to the B feature, as the Mo valence increases from 4+ to 6+. Moreover, as the oxidation state of the Mo increases, the centrum of the combined A−B features exhibits a chemical shift to higher energy. The $Sr_3FeMoO_{6.88}$ $L_{2,3}$ spectra are intermediate

(28) Lindén, J.; Yamamoto, T.; Karppinen, M.; Yamauchi, H.; Pietari, T. *Appl. Phys. Lett.* **2000**, *76*, 2925.

(29) Zeng, Z.; Greenblatt, M.; Sunstrom, J. E., IV; Croft, M.; Khalid, S. *J. Solid State Chem.* **1999**, *147* (1), 185.

(30) Zeng, Z.; Fawcett, I. D.; Greenblatt, M.; Croft, M. *Mater. Res. Bull.* **2001**, *36*, 705.

(31) Veith, G. M.; Greenblatt, M.; Croft, M.; Goodenough, J. B. *Mater. Res. Bull.* **2001**, *36* (7−8), 1521.

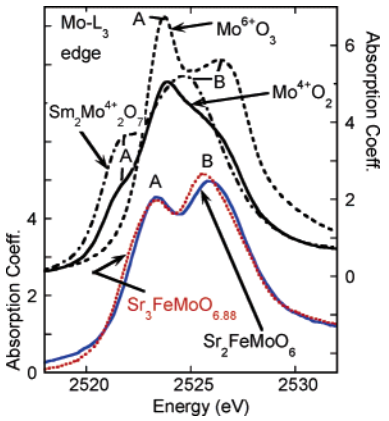

Figure 9. Mo−L_3 edge XANES data.

between the Mo^{4+} and Mo^{6+} standards and are very similar to the spectra of the Mo^{5+} double perovskite Sr_2FeMoO_6. The $Sr_3FeMoO_{6.88}$ $L_{2,3}$ spectra reflect the additional splittings of the t_{2g} and e_g orbitals in the tetragonal (or square pyramidal at the O-vacancy sites) ligand field. Specifically, the narrower A−B peak splitting, a subtle low-energy shoulder on the A-feature and a high-energy shoulder on the B-feature, should be noted. The small chemical shift, to lower energy of the $Sr_3FeMoO_{6.88}$ spectra, relative to the Sr_2FeMoO_6 spectra indicates a slightly lower Mo valence. Thus, the combined Fe and Mo XANES support $Fe^{3+}/Mo^{4+/5+}$ formal oxidation states in $Sr_3FeMoO_{6.88}$, which is consistent with the magnetic and Mössbauer results.

6. Electrical Resistivity. The resistivity for $Sr_3FeMoO_{6.88}$, Figure 10, displays semiconducting behavior, with a room-temperature resistivity of $\rho_{RT} \sim 0.05$ Ω-cm, which is close to that reported for Sr_3FeMoO_6 double perovskite (0.03 Ω-cm).[10] The temperature dependence of resistivity cannot be fitted either by an activated or a variable range hopping (VRH) mechanism in the entire T range, and this can indicate either different mechanisms of transport in different temperature ranges or some mechanism beyond simple activated or VRH scenarios. Assuming that the activated law is valid at high T (220−350 K), the activation energy of conduction, E_a, was estimated as 0.038 eV. The magnitude of MR (Figure 10 bottom) increases with decreasing temperature and reaches the value of −15% at 5 K in an applied field of 5 T, which is significantly lower than that of the double perovskite Sr_2FeMoO_6 (42% at 4.2 K and 7 T).[10] The onset of MR coincides with the 270 K susceptibility upturn. Accordingly, the effect could be attributed either to the intrinsic MR of the intergrowth phase ($n \neq 2$ RP) or to a phenomenon similar to the giant MR (GMR) observed in magnetic multilayer thin films.

Conclusions

A new oxygen-deficient $n = 2$ Ruddlesden−Popper-type compound, $Sr_3FeMoO_{6.88}$, was synthesized by solid-state reaction in an evacuated quartz tube.

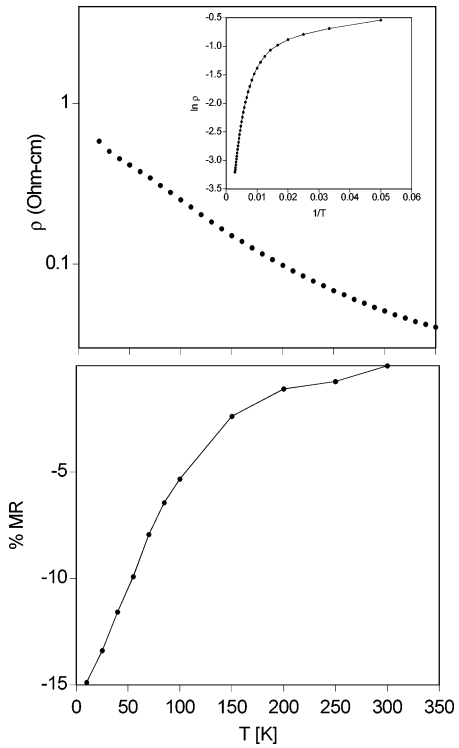

Figure 10. Top: Resistivity as a function of temperature of $Sr_3FeMoO_{6.88}$. (Inset: top, plot of ln ρ vs $1/T$). Bottom: % MR as a function of T measured in an applied field of 5 T.

The $n = 2$ RP phase only forms (under the conditions tried here) with an anion deficient structure in contrast to the double perovskite which is reported to be stoichiometric. $Sr_3FeMoO_{6.88}$ forms with a disordered Fe/Mo structure in stark contrast to the completely ordered Fe−Mo arrays in the double perovskite. $Sr_3FeMoO_{6.88}$ and Sr_2FeMoO_6 both exhibit semiconducting-like behavior with room-temperature resistivities of 0.05 and 0.03 Ω-cm, respectively.[10] Both phases exhibit magnetoresistance commensurate with magnetic ordering; however, the long-range magnetic order and temperatures are significantly different: AFM at 85 K for $Sr_3FeMoO_{6.88}$ versus FM at 410 K[9] for the analogous double perovskite. XANES and Mössbauer data are consistent with Fe^{3+} and mixed Mo^{4+} and Mo^{5+} formal oxidation states.

Acknowledgment. We thank Dr. James Richardson and Evan Maxey at the IPNS, Argonne National Laboratory for collecting the PND data. In addition, we are grateful to Prof. W. H. McCarroll and Drs. Peter Kalifah and Maxim Lobanov for their critical reading of this manuscript and Dr. Barbara McKernan-Veith for her editorial assistance. This work was supported by the NSF-Solid State Chemistry Grants DMR 99-07963 and DMR 02-33697.

Supporting Information Available: Powder data table and PXD plot for $Sr_3FeMoO_{6.88(1)}$. This material is available free of charge via the Internet at http://pubs.acs.org.

CM048839R